第 42 卷 第 18 期/2022 年 9 月/光学学报 特邀论文

光学学报

Experimental Evaluation of Temperature Dependence of Pure Water Absorption Coefficient in Near-Infrared Domain

Chen Liangfeng[1], Lee Zhongping[1,2*], Lin Gong[1], Wang Yongchao[1], Wang Junwei[1], Lai Wendian[1]

[1]*State Key Lab of Marine Environmental Science, College of Ocean and Earth Sciences, Xiamen University, Xiamen* 361005, *Fujian, China;*

[2]*School for the Environment, University of Massachusetts Boston, Boston* 02125, *MA, USA*

Abstract There are many reports regarding the impact of temperature (T) on the absorption coefficient of pure water [$a_w(\lambda)$] in the literature, and some of them are not consistent. In this study, using well-controlled measurements of remote-sensing reflectance [$R_{rs}(\lambda)$] of highly turbid waters where the temperature varied from 7 to 51 ℃, we analyzed the changes in the shape of R_{rs} in the 740-850 nm domain, especially the relationship between this change in R_{rs} spectral shape and the change of spectral shape in $a_w(\lambda)$ caused by temperature variations indicated by the latest laboratory measurements from Rottgers *et al*. We found that the twist of R_{rs} spectral shape in the 740-850 nm domain can be well explained by the twist of spectral shape in $a_w(\lambda)$ caused by changes in temperature. Since the spectral shape of R_{rs} in the near infrared (NIR) is mainly driven by the spectral variation of $a_w(\lambda)$, the consistency provides an independent verification of the spectrally-opposite temperature dependence of $a_w(\lambda)$ for bands in the 740-850 nm domain that was obtained from laboratory settings.

Key words ocean optics; pure water; absorption coefficient; temperature dependence; near-infrared

纯水吸收系数在近红外波段随温度变化的实验评估

陈粮峰[1]，李忠平[1,2*]，林供[1]，汪永超[1]，王俊炜[1]，赖文典[1]

[1]厦门大学近海海洋环境科学国家重点实验室，厦门大学海洋与地球学院，福建 厦门 361005；

[2]马萨诸塞州立大学波士顿分校环境学院，马萨诸塞州 波士顿 02125，美国

摘要 关于温度(T)对纯水吸收系数[$a_w(\lambda)$]的影响，文献中有许多报道，其中有些报道并不一致。在这项研究中，通过对温度从7 ℃到51 ℃变化的高浑浊水体的遥感反射比[$R_{rs}(\lambda)$]的测量，分析了R_{rs}光谱在740～850 nm波段的形状变化，特别是R_{rs}与最近Rottgers等在实验室测量所揭示的由温度变化引起的$a_w(\lambda)$光谱形状变化的关系。分析发现R_{rs}光谱在740～850 nm波段的形状扭曲可以很好地由温度变化引起的$a_w(\lambda)$光谱的形状扭曲来解释。由于在近红外(NIR)波段R_{rs}光谱的形状主要由$a_w(\lambda)$光谱来决定，因此该结果的一致性提供了对从实验室测量获得的740～850 nm波段$a_w(\lambda)$数值与温度呈相反依赖性的独立验证。

关键词 大气光学；纯水；吸收系数；温度依赖性；近红外

中图分类号 TN929.11 **文献标志码** A **DOI**: 10.3788/AOS202242.1801007

1 Introduction

The spectral absorption coefficient of pure water [a_w, cm^{-1}] is a basic inherent optical property (IOP)[1], which characterizes the capacity of pure water to absorb light. It plays an important role in regulating the propagation

收稿日期：2022-04-10；**修回日期**：2022-05-21；**录用日期**：2022-05-25

基金项目：国家自然科学基金重点项目（41830102）

通信作者：*zpli2015@xmu.edu.cn

of solar radiation in aquatic environment as well as heating of the upper water column, which is also a critical optical property applied in the calibration of *in situ* absorption sensors[2-3] and utilized in the "black" pixel assumption in atmosphere correction[4].

Many studies in the past have shown that the a_w has two distinct characteristics. On the one hand, the values of a_w vary enormously from UV-visible to near-infrared, spanning several orders of magnitude[5-6]. On the other hand, due to difficulties in the preparation of "pure" water and in meeting the high sensitivity requirement of instrument to measure this optical property, there are also large variations of reported a_w values in the literature[7-11], and even from the same laboratory[14-15].

Further, it has also been indicated that the values of a_w depend on environmental influences, such as temperature (T) and salinity[14-15], but the reported dependence on temperature in the literature also varies. For instance, for wavelengths in the 350-500 nm range, Pegau *et al.*[16] found that a_w increases with T, while Röttgers *et al.*[14] found it slightly decreases with T. Recently, using ~20 years of satellite data measured at the ocean gyres, Wei *et al.*[5] found that the impact of temperature on a_w in the blue bands is consistent with that reported in Röttgers *et al.*[14]. For the temperature dependence of a_w in the near-infrared (NIR) domain, Röttgers *et al.*[14] indicated spectrally opposite impacts (see Fig. 1), where a_w increased with T between 740 nm and 835 nm, but decreased with T between 795 nm and 890 nm. However, for such spectral behaviors, there are no independent, out-of-laboratory measurements, to verify the results.

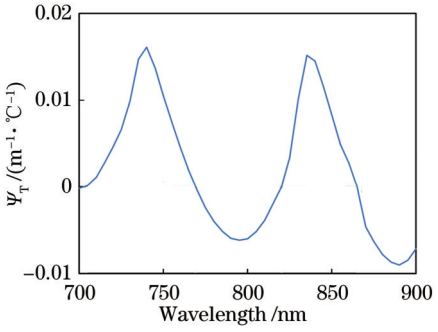

Fig. 1 Temperature correction coefficient Ψ_T for a_w obtained from Rottgers *et al.*[14] in the wavelength range of 700-900 nm

Laboratory measurement of a_w is not an easy task[12,14]. It requires very careful preparation of the sample - "pure" water[17-18], as well as sensitive and well calibrated instrumentation[13]. In particular, when the objective is to study the impact of T on a_w, the impact of T on the measurement system has to be shielded off also, and otherwise artifacts could be introduced to the impact of T on a_w, which could be an important source of the different temperature dependences reported in the literature.

In this study, to avoid the above-mentioned difficulties in laboratory measurements, we use remote-sensing reflectance [$R_{rs}(\lambda)$, sr^{-1}] of highly turbid waters in the NIR to analyze the response of a_w to different temperatures. This is based on that R_{rs} is in general a function of $b_b/(a+b_b)$, where b_b is the total backscattering coefficient and a is the total absorption coefficient. For the NIR domain, the absorption coefficient of gelbstoff can be ignored, and a can be expressed as the following after considering T-dependent a_w,

$$a(\lambda, T) = a_w(\lambda, T_0) + \Psi_T(\lambda)(T - T_0) + a_p(\lambda), \quad (1)$$

where T_0 is the reference temperature (set as 20 ℃), Ψ_T is the temperature correction coefficient of a_w, and a_p is the absorption coefficient of particulates. Since the scattering contribution from pure water can be ignored for turbid waters, R_{rs} in the NIR can be approximated as[19-20]

$$R_{rs}(\lambda) = G\frac{b_{bp}(\lambda)}{a_w(\lambda, T_0) + \Psi_T(\lambda)(T - T_0) + a_p(\lambda) + b_{bp}(\lambda)}, \quad (2)$$

where b_{bp} is the backscattering coefficient of suspended particles, while G is the model coefficient, which in the first order approximates 0.05 sr^{-1}. In the NIR domain, the spectral shapes of both a_p and b_{bp} are flat and do not show spectrally selective temperature dependences. Thus if the dependence of a_w in NIR at difference wavelengths is opposite, we should expect to see a twist of R_{rs} spectral shapes in the NIR (740-850 nm here, more specifically).

To analyze this response of a_w on temperature, we thus carried out controlled experiments to measure hyperspectral R_{rs} of very turbid waters at different temperatures. A high turbidity is required to obtain adequate R_{rs} measurements in the NIR domain, where the values of a_w are very high[21], and thus it is required to have high b_{bp} (which is driven by sediments or turbidity) to ensure adequate R_{rs} signal in the NIR. The following of this article then describes the experimental settings and the results obtained.

2 Methods and Setups

2.1 Measurement Setups

To evaluate the impact of temperature on a_w in the NIR (740-850 nm) domain, we designed an outdoor experimental system to measure R_{rs} of highly turbid

waters under controlled temperature. It includes a large black customized tank (see Fig. 2) with a height of 0.6 m and a diameter of 2.2 m to contain turbid waters. This tank was placed on an empty area on the campus of Xiamen University in China, where there were no objects in the nearby to block the radiation from the sun and sky. Water from a nearby lake was used to fill the tank, and a large amount of fine sediments were added to obtain highly turbid water. Gentle stirring of this water-sediment mixture was carried out to keep it well mixed and that the sediments not sunk quickly.

Fig. 2 Photo of the water-filled tank along with the radiometer when taking measurement of L_t via above-water approach (AWA)

The temperature of this water-sediment mixture was adjusted by adding a large number of crushed ice cubes and heating rods, which resulted in a temperature range of 7 to 51 ℃. The temperature of the water body was measured simultaneously from five different spots near the surface when radiometric measurements were taken, where the temperature resolution was 0.1 ℃, which is sufficient for this study. An average of the temperature readings from the five spots was used to represent the temperature for each set of radiometric measurements.

The experiments were carried out on 4 December and 13 December, 2021 between 10:00 and 14:00, under cloudless blue-sky day and low wind. The impacts of the tank wall and tank bottom on the water-leaving radiance at the center of this tank are negligible as the Secchi disk depth is ~0.15 m after adding high loads of sediments into such lake waters.

2.2 Instrument and Approach to Measure R_{rs}

To obtain R_{rs} in the NIR, the spectrometer (SE SR1901) of Spectral Evolution (USA) was used to collect the required radiance. SE SR1901 has a wavelength range of 280-1900 nm, with a spectral resolution of ~2 nm and a field of view of 4°. The spectrometer has two probes, one is with a cosine collector used for measuring downwelling irradiance, the other is used for measuring radiance, and both are factory calibrated where their equivalent radiation noises are orders lower than the radiance to be measured in this study. In order to avoid potential mismatch in radiometric and spectral calibrations between the two probes, we just used the probe for radiance, and the downwelling irradiance was calculated from measuring the radiance reflected from a standard gray card, which has a reflectance of 20%.

For such controlled environment, we took the AWA[22-24] to measure the total upwelling radiance (L_t) and the sky radiance (L_{sky}) in the reciprocal angle of L_t for the determination of water-leaving radiance (L_w) that is required for the calculation of R_{rs}. The angular geometry[22] for the measurement of L_t is 40° from nadir with an azimuth angle of 135° away from the sun. The radiance leaving a standard gray card (L_{plaque}) was measured using the same spectrometer. From these measurements, R_{rs} was calculated as follows[25]:

$$R_{rs}(\lambda)=\frac{\rho}{\pi}\frac{L_t(\lambda)-FL_{sky}(\lambda)}{L_{plaque}(\lambda)}-\Delta, \tag{3}$$

where ρ is the reflectance (0.2) of the gray card, F is the Fresnel reflectance of the air-sea surface and takes a value of 0.023 because we restrict the measurements to cloudless and calm water conditions. Δ reflects a residual correction of surface-reflected radiance that might not be completely corrected from the subtraction of FL_{sky}, and is determined by setting the average value of R_{rs} (1600-1650 nm) to 0 based on Lee *et al.*[6], since SE SR1901 covers wavelength up to 1980 nm.

2.3 Measurement

We first added a large amount of crushed ice to the turbidity water. Gentle stirring was carried out to make the ice melted and the water well mixed. After no floating ice visible on the water surface, we recorded the temperature and measured L_t, L_{sky}, and L_{plaque} in turn via AWA. Each property was measured 10 times to ensure stable and reliable data. After that, the water was gradually warmed, and generally it took ~40 minutes for each increase of 10 ℃. The temperature range of liquid water in the nature environment is about −2-30 ℃, but we expand the higher end to 51 ℃ in order to more clearly observe the impact of temperature on a_w. Finally, we took radiometric measurements at 14 different temperatures, which were 7, 10, 12, 15, 17, 20, 25, 27, 29, 32, 37, 42, 47, and 51 ℃. For each temperature scale, it took approximately 2 minutes to complete the measurement cycle, where the ambient light field could be considered stable and the variation of water temperature was within ~0.5 ℃, and thus it is appropriate to consider these measurements were completed under the "same" environmental conditions and the "same" temperature.

In addition, we also collected water samples from the

surface to measure the IOPs of the water-sediment mixture, which include the absorption coefficients of suspended particles (a_p) and gelbstoff (a_g) that corresponding to each set of R_{rs} measurement at different temperatures. The absorption coefficients of the water samples were all measured with a dual-beam PE Lambda 950 spectrophotometer equipped with an integrating sphere (150 mm in diameter) in the laboratory. The spectrum of a_p was measured by the transmittance-reflectance (T-R) method[26] after the water sample was filtered by GF/F filters for 30 mL following the filter-pad technique[27] and a_g spectrum was measured according to the method from Bricaud *et al*.[28].

3 Results and Discussion

3.1 R_{rs} of Tank Waters

The resulted R_{rs} spectra at different temperatures obtained on 4 December, 2021 are presented in Fig. 3(a), where the lowest temperature was 7 ℃ and the highest temperature was 29 ℃, while Fig. 3(b) shows R_{rs} spectra obtained on 13 December, 2021, with temperature varied from 17 ℃ to 51 ℃. Overall, the values (the averaged coefficient of variation is less than 2%) of the measured R_{rs} are in a range of 0.005-0.03 sr^{-1} for the spectral window of 700-900 nm, which are similar to those of high-sediment-load waters of the Changjiang River estuary[6], so do the spectral shapes of these measured R_{rs}. These characteristics indicate that the obtained R_{rs} spectra indeed are those of high sediment waters. Note that while gentle stirring of the water-sediment mixture was carried out for each set of measurements, it cannot guarantee it is the same kind of water-sediment mixture for each radiometric measurement, thus not surprise to observe variations in the R_{rs} values. This is also evidenced by the absorption spectra of the particulates (see Fig. 4) obtained from the water samples, where a_p (700-900 nm) changed a lot for water samples collected under different temperature. However, as presented and discussed below, the key is the spectral curvature of $R_{rs}(\lambda)$ in the 700-900 nm range, and thus the minor variations of $R_{rs}(\lambda)$ values are acceptable for this study.

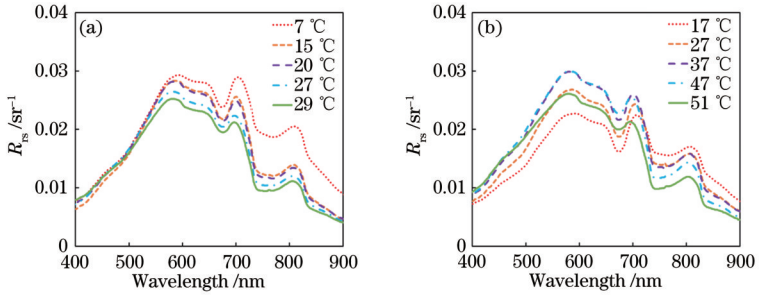

Fig. 3 R_{rs} spectra at different temperatures obtained in this study. (a) Measured on 4 December, 2021; (b) measured on 13 December, 2021

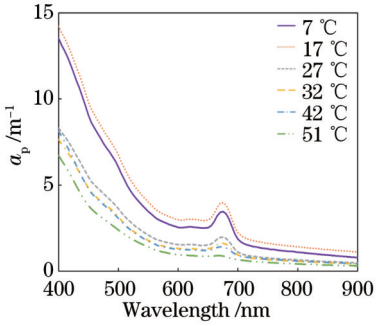

Fig. 4 a_p spectra of the water-sediment mixture at different temperature (or time) of this study

3.2 Relationship Between R_{rs}(NIR) Spectral Shape and Temperature

To highlight the variation of R_{rs} spectral shape in the NIR, all R_{rs} spectra under different T are normalized to $R_{rs}(770)$, represented as $R_{rs\_Nor}(\lambda)$:

$$R_{rs\_Nor}(\lambda)=\frac{R_{rs}(\lambda)}{R_{rs}(770)}. \tag{4}$$

The reason to select 770 nm as the reference point is that $a_w(770)$ is insensitive to T (see Fig. 1)[1,17]. The resulted R_{rs_Nor}(NIR) spectra are presented in Fig. 5. Because $a_w(740)$ [and $a_w(835)$] increases with T and $a_w(795)$ decreases with T, we should expect a twist of R_{rs_Nor} between 740 nm and 795 nm, which is clearly shown in Fig. 5, where $R_{rs\_Nor}(740)$ [and $R_{rs\_Nor}(835)$] decreases with the increase of T, but the opposite is

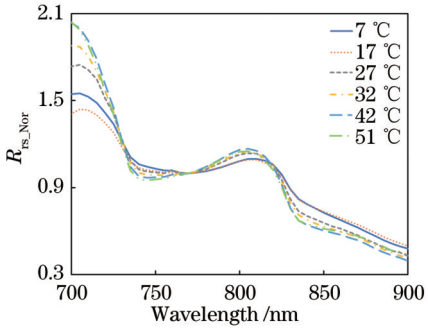

Fig. 5 Normalized R_{rs} spectra R_{rs_Nor} at different temperatures

observed for $R_{rs\_Nor}(795)$. Further, there is another "standing" point at ~820 nm where $R_{rs\_Nor}(820)$ is found nearly insensitive to T, which is consistent with $\Psi_T(820)$ as 0[14,17].

The opposite responses of $R_{rs}(\lambda_1)$ and $R_{rs}(\lambda_2)$ to the change of T were further quantitatively analyzed by the relative difference ($D_{R_{rs}}$) between $R_{rs}(\lambda_1)$ and $R_{rs}(\lambda_2)$, calculated as:

$$D_{R_{rs}}(\lambda_1:\lambda_2)=\frac{R_{rs}(\lambda_1)-R_{rs}(\lambda_2)}{R_{rs}(\lambda_1)+R_{rs}(\lambda_2)}. \tag{5}$$

For comparison, we also calculated the relative difference between $a_w(\lambda_1)$ and $a_w(\lambda_2)$ (D_{aw}) for these temperatures:

$$D_{aw}(\lambda_1:\lambda_2)=\frac{a_w(\lambda_1)-a_w(\lambda_2)}{a_w(\lambda_1)+a_w(\lambda_2)}=\frac{\left[a_w(\lambda_1,T_0)-a_w(\lambda_2,T_0)\right]+\left[\psi_T(\lambda_1)-\psi_T(\lambda_2)\right](T-T_0)}{\left[a_w(\lambda_1,T_0)+a_w(\lambda_2,T_0)\right]+\left[\psi_T(\lambda_1)+\psi_T(\lambda_2)\right](T-T_0)}, \tag{6}$$

where the values of $a_w(\lambda_i, T_0)$ (i=1, 2) were taken from Kou *et al.*[21] for 725-900 nm, while values of Ψ_T were taken from Rottgers *et al.*[14]. Note that this relative difference is a measure of the spectral curvature of R_{rs} and a_w, respectively.

Fig. 6(a) shows the changes of $D_{R_{rs}}$ and D_{aw} (λ_1 as 740 nm and λ_2 as 795 nm) for T in a range of 7-51 ℃. For this temperature range, $D_{aw}(740:795)$ increased from ~0.03 to 0.20, this twist of a_w shape is expected based on Eq. 1 and the values of Rottgers *et al.*[14]. On the other hand, $D_{R_{rs}}(740:795)$ decreased from ~0 to −0.09, indicating a relatively narrower change of $D_{R_{rs}}(740:795)$ compared to $D_{aw}(740:795)$. This reduced range of $D_{R_{rs}}(740:795)$ is due to the impact of a_p (see Eq. 1), which has a high value for the water-sediment mixture of this study even at NIR bands (see Fig. 4). Although the spectral shape of a_p does not change with T, because R_{rs} is a measure of the total absorption, thus the high a_p value dampens the change of $D_{R_{rs}}(740:795)$.

The opposite relationships with T for $D_{aw}(740:795)$ and $D_{R_{rs}}(740:795)$ basically reflect that R_{rs} is inversely related to the absorption coefficient (see Eq. 2). To highlight the change of $D_{R_{rs}}(740:795)$ due to the change of a_w with T, Fig. 6(b) shows a scatterplot between $D_{R_{rs}}(740:795)$ and $D_{aw}(740:795)$, where the correlation coefficient r between the two is −0.98, which highlights the significant cause and effect relationship between R_{rs} and a_w.

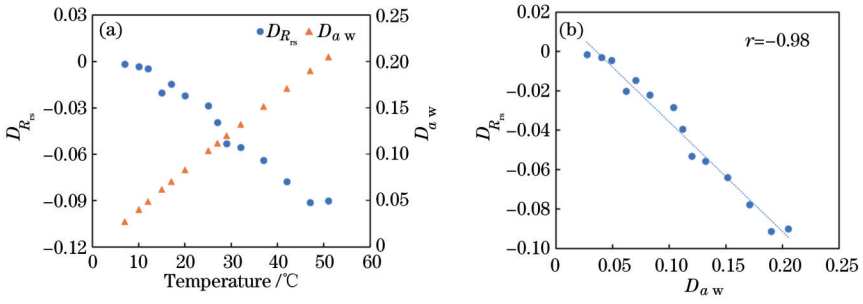

Fig. 6 Relationship between $D_{R_{rs}}$ and D_{aw} (λ_1 as 740 nm and λ_2 as 795 nm). (a) Change of $D_{R_{rs}}$ and D_{aw} for T in a range of 7-51 ℃; (b) scatterplot between $D_{R_{rs}}(740:795)$ and $D_{aw}(740:795)$

Similar results were found for $D_{R_{rs}}$ and D_{aw} of the wavelength pair 795 nm and 835 nm, but this time D_{aw} decreases with temperature, and thus $D_{R_{rs}}$ increases with temperature [see Fig. 7(a)]. As Fig. 6(b),

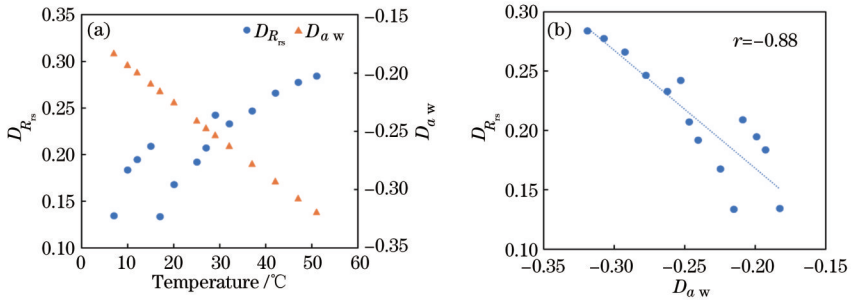

Fig. 7 Relationship between $D_{R_{rs}}$ and D_{aw} (λ_1 as 795 nm and λ_2 as 835 nm). (a) Changes of $D_{R_{rs}}$ and D_{aw} for T in a range of 7-51 ℃; (b) scatterplot between $D_{R_{rs}}$ (795 nm/835 nm) and D_{aw} (795 nm/835 nm)

Fig. 7(b) shows the scatterplot between D_{aw}(795:835) and $D_{R_{rs}}$(795:835), with an r value as −0.88, also very significant. The reason for this slightly lower r value compared to the correlation between D_{aw}(740:795) and $D_{R_{rs}}$(740:795) is not clear yet, likely due to sharp changes of R_{rs} for wavelengths around 835 nm (see Fig. 3), and thus a resolution of the sensor could impact the results. Also, R_{rs}(835) is much lower than R_{rs}(795), and a slight error in the measurement of R_{rs} will thus impact more on $D_{R_{rs}}$(795:835). Nevertheless, the strong correlation (0.88 and higher) between the $D_{R_{rs}}$ and D_{aw} provides a clear support about the wavelength dependence of a_w obtained by Rottgers *et al.*[14] for these bands.

Because R_{rs} is also related to b_{bp} and a_p (see Eq. 2), some changes of $D_{R_{rs}}$ could be a result of the changes of b_{bp} and/or a_p. To evaluate these potentials, the change of $D_{R_{rs}}$ caused by changes of a_p and b_{bp} are shown in Fig. 8, where the value of a_w is kept as that at 20 ℃. For the wide changes of a_p [(a_p(740) in a range of ~0.5-1.5 m^{-1}] and b_{bp} [b_{bp}(555) in a range of 0.1-1.0 m^{-1}], it is found that $D_{R_{rs}}$(740:795) is in a range of −0.075 to −0.069, a range significantly narrower than the change of $D_{R_{rs}}$(740:795) under different temperatures (see Fig. 8). Thus it is safe to conclude that the changes of $D_{R_{rs}}$(740:795) [and $D_{R_{rs}}$(795:835)] measured for different temperatures were driven by changes of D_{aw}.

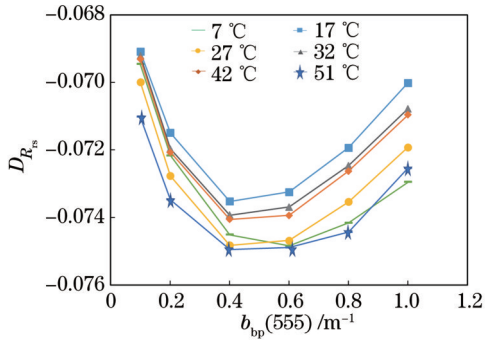

Fig. 8 Change of $D_{R_{rs}}$ caused by changes of a_p and b_{bp}

4 Conclusions

From the measured R_{rs} of highly turbid waters under different temperature, it is clear that the change of spectral curvature of R_{rs} in the 740-850 nm range is driven by the spectrally varying change of a_w at different temperatures. More importantly, this change in R_{rs} shape is consistent with that predicted by the latest laboratory measurements of Rottgers *et al.*[14]. Therefore, this experiment and results provide an independent evaluation and confirmation of the spectrally opposite impact of temperature on a_w, which further provide confidence on using the Ψ_T, at least in the 740-850 nm range of Rottgers *et al.*[14], in field measurements and/or satellite ocean color data processing. However, because the a_w values for wavelengths longer than 900 nm are extremely high, although the Ψ_T values are even higher for some wavelengths longer than 900 nm (Rottgers *et al.*[14]), our system may not be sensitive enough to measure the change of R_{rs} shape for those longer wavelengths, and thus the Ψ_T values of these bands still wait to be confirmed.

References

[1] Preisendorfer R W. Hydrologic optics[M]. Honolulu: US Department of Commerce, National Oceanic and Atmospheric Administration, Environmental Research Laboratories, Pacific Marine Environmental Laboratory, 1976.

[2] Sullivan J M, Twardowski M S, Zaneveld J R V, et al. Hyperspectral temperature and salt dependencies of absorption by water and heavy water in the 400-750 nm spectral range[J]. Applied Optics, 2006, 45(21): 5294-5309.

[3] Moore C C. WET labs ac-9: field calibration protocol, deployment techniques, data processing, and design improvements[J]. Proceedings of SPIE, 1997, 2963: 1-6.

[4] Gordon H R. Removal of atmospheric effects from satellite imagery of the oceans[J]. Applied Optics, 1978, 17(10): 1631-1636.

[5] Wei G M, Lee Z P, Wu X L, et al. Impact of temperature on absorption coefficient of pure seawater in the blue wavelengths inferred from satellite and *in situ* measurements[J]. Journal of Remote Sensing, 2021(1): 289-301.

[6] Lee Z P, Shang S L, Lin G, et al. On the modeling of hyperspectral remote-sensing reflectance of high-sediment-load waters in the visible to shortwave-infrared domain[J]. Applied Optics, 2016, 55(7): 1738-1750.

[7] Morel A. Optical properties of pure water and pure sea water[J]. New York: Academic Press, 1974: 1-24.

[8] Buiteveld H, Hakvoort J, Donze M. Optical properties of pure water[J]. Proceedings of SPIE, 1994, 2258: 1-10.

[9] Lee Z P, Wei J W, Voss K, et al. Hyperspectral absorption coefficient of "pure" seawater in the range of 350-550 nm inverted from remote sensing reflectance[J]. Applied Optics, 2015, 54(3): 546-558.

[10] Patel C K N, Tam A C. Optical absorption coefficients of water[J]. Nature, 1979, 280(5720): 302-304.

[11] Querry M R, Cary P G, Waring R C. Split-pulse laser method for measuring attenuation coefficients of transparent liquids: application to deionized filtered water in the visible region[J]. Applied Optics, 1978, 17(22): 3587-3592.

[12] Pope R M, Fry E S. Absorption spectrum (380-700 nm)

of pure water. II. Integrating cavity measurements[J]. Applied Optics, 1997, 36(33): 8710-8723.

[13] Mason J D, Cone M T, Fry E S. Ultraviolet (250–550 nm) absorption spectrum of pure water[J]. Applied Optics, 2016, 55(25): 7163-7172.

[14] Röttgers R, McKee D, Utschig C. Temperature and salinity correction coefficients for light absorption by water in the visible to infrared spectral region[J]. Optics Express, 2014, 22(21): 25093-25108.

[15] Pegau W S, Gray D, Zaneveld J R. Absorption and attenuation of visible and near-infrared light in water: dependence on temperature and salinity[J]. Applied Optics, 1997, 36(24): 6035-6046.

[16] Pegau W S, Zaneveld J R V. Temperature dependence of the absorption coefficient of pure water in the visible portion of the spectrum[J]. Proceedings of SPIE, 1994, 2258: 597-604.

[17] Langford V S, McKinley A J, Quickenden T I. Temperature dependence of the visible-near-infrared absorption spectrum of liquid water[J]. The Journal of Physical Chemistry A, 2001, 105(39): 8916-8921.

[18] Quickenden T I, Irvin J A. The ultraviolet absorption spectrum of liquid water[J]. The Journal of Chemical Physics, 1980, 72(8): 4416-4428.

[19] Gordon H R, Brown O B, Evans R H, et al. A semianalytic radiance model of ocean color[J]. Journal of Geophysical Research: Atmospheres, 1988, 93(D9): 10909-10924.

[20] Nechad B, Ruddick K G, Park Y. Calibration and validation of a generic multisensor algorithm for mapping of total suspended matter in turbid waters[J]. Remote Sensing of Environment, 2010, 114(4): 854-866.

[21] Kou L, Labrie D, Chylek P. Refractive indices of water and ice in the 0.65- to 2.5-μm spectral range[J]. Applied Optics, 1993, 32(19): 3531-3540.

[22] Mobley C D. Estimation of the remote-sensing reflectance from above-surface measurements[J]. Applied Optics, 1999, 38(36): 7442-7455.

[23] Mueller J L. Ocean optics protocols for satellite ocean color sensor validation, revision 4: radiometric measurements and data analysis protocols[M]. New York: NASA, 2003.

[24] Mueller J L, Davis C, Arnone R, et al. Above-water radiance and remote sensing reflectance measurement and analysis protocols[J]. Radiometric Measurements and Data Analysis, Ocean Optics Protocols For Satellite Ocean Color Sensor, Validation, Revision, 2003, 4: 21-30.

[25] Lee Z P, Ahn Y H, Mobley C, et al. Removal of surface-reflected light for the measurement of remote-sensing reflectance from an above-surface platform[J]. Optics Express, 2010, 18(25): 26313-26324.

[26] Tassan S, Ferrari G M. Variability of light absorption by aquatic particles in the near-infrared spectral region[J]. Applied Optics, 2003, 42(24): 4802-4810.

[27] Kiefer D A, SooHoo J B. Spectral absorption by marine particles of coastal waters of Baja California[J]. Limnology and Oceanography, 1982, 27(3): 492-499.

[28] Bricaud A, Morel A, Prieur L. Absorption by dissolved organic matter of the sea (yellow substance) in the UV and visible domains[J]. Limnology and Oceanography, 1981, 26(1): 43-53.